4 Chapter: 2-(Diarylalkyl)Aminobenzothiazole Derivatives Induce Autophagy and Apoptotic Death Through SIRT Inhibition and P53 Activation in MCF7 Breast Cancer Cells

4.1 Introduction:

Breast cancer (BC) is the primary cause of cancer-related mortality among women because of its morbidity and mortality at high rates; its propensity to spread to the liver, lungs, bone marrow, and lymph nodes complicates anti-tumor treatment [201]. Considerable progress has been achieved in enhancing therapeutic approaches and comprehending the molecular pathways behind breast cancer. Nevertheless, metastasis continues to pose a significant obstacle to therapeutic treatment, and the precise processes underlying it remain unclear [202]. Despite significant progress in treatment options, many patients with BC continue to experience poor outcomes. This in turn has a significant influence on their lives and highlights an imperative requirement to progress innovative approaches for breast cancer treatment [203].

The family of NAD^+-dependent class III HDACs known as sirtuins (SIRTs) has seven homologues in mammals, some of which have monoribosyltransferase activity and others that have HDAC activity [59]. SIRTs target histones and other non-histone proteins in distinct subcellular sites, and they have varied locations throughout the cell: SIRT2 is mostly cytosolic, SIRT3, SIRT4, and SIRT5 are located in the mitochondria, and SIRT1, SIRT6, and SIRT7 are mainly found in the nucleus [204]. Because of their unique subcellular distribution, sirtuins can influence particular cellular functions within their compartments. For instance, cytosolic SIRT2 affects cell cycle progression and cytoskeletal dynamics, nuclear SIRT1 controls gene expression and DNA repair, and mitochondrial SIRT3 preserves metabolic balance and oxidative stress responses [205-207]. SIRT1 can modify cell viability by controlling several proteins and can cause chromatin silencing by deacetylating histones H1, H3, and H4 [208-213]. Since SIRT1-mediated deacetylation of Lys382 within p53 has been demonstrated to promote

apoptosis, the possible involvement of SIRT1 in cancer biology was initially suggested when p53 was discovered to be a direct substrate [214, 215]. SIRT2 is significantly expressed in human basal-like breast cancer (BLBC), which confers basal-like malignant characteristics and development by preventing Slug from being deacetylated [216]. For many non-histone protein substrates, including CDK9, HIF-1α, Slug, K-Ras4a, and FOXO3, SIRT2 can catalyze deacetylation [214, 217]. In breast cancer, SIRT3 contributes to carcinogenesis, and the expression levels differ within the same breast or mammary cancers [164, 218]. Drug-resistant breast cancer cells have increased levels of SIRT3 expression. The sensitivity of drug-resistant cells is enhanced by SIRT3 knockdown, which also caused apoptosis and raised the amounts of ERβ and ROS in the mitochondria [219].

Recent research suggests that the process of autophagic death is essential for controlling cell death in breast cancer cells that have gained resistance to different therapies [220-223]. The catabolic process of autophagy involves the sequestration of cytoplasmic proteins and organelles in vacuoles, which are then transported to lysosomes for recycling and breakdown [224, 225]. Autophagy induction has also been noted in cancerous cells after histone deacetylase (HDAC) inhibitor therapy [226].

In many pharmaceutically active chemicals, benzothiazole, a class of nitrogen and sulfur compounds, has one of the most significant and preferred ring configurations. In this context, 2-aminobenzothiazoles are a significant heterocyclic ring with a broad range of medicinal uses because of their structural variety [227]. Amino benzothiazole has attracted a lot of attention lately because of its pharmacological properties, which include analgesic, antifungal, anticonvulsant, anti-inflammatory, and anticancer effects [228, 229]. The stability of the molecule-receptor complex is said to be significantly influenced

by the polarized character of nitrogen-containing heterocyclic rings, such as amino benzothiazole. In general, it creates an optimal contact that results in anticancer actions, increasing the stability of the complex [230].

In this study, we explored the anticancer effect of 2-(diarylalkyl) amino benzothiazole derivatives, **7**ab and **7**ba and underlying molecular mechanisms of action on breast cancer cells. We first established that **7**ab and **7**ba exhibit potent anti-cancer activities. Then we explored its mechanism of action, revealing that molecules **7**ab, **7**ba function as SIRT1 inhibitors. Molecules **7**ab and **7**ba have an inhibitory effect on SIRT1 and affect the tumor suppressor p53, specifically its acetylation status. Our results demonstrated that **7**ab and **7**ba not only triggered apoptotic cell death but also elevated LC3-II levels, indicating the accumulation of autophagosomes and autophagic type II cell death. These findings suggest that **7**ab and **7**ba hold promising therapeutic potential for breast cancer, as they act by inducing both the cell death mechanisms, i.e., autophagy and apoptosis.

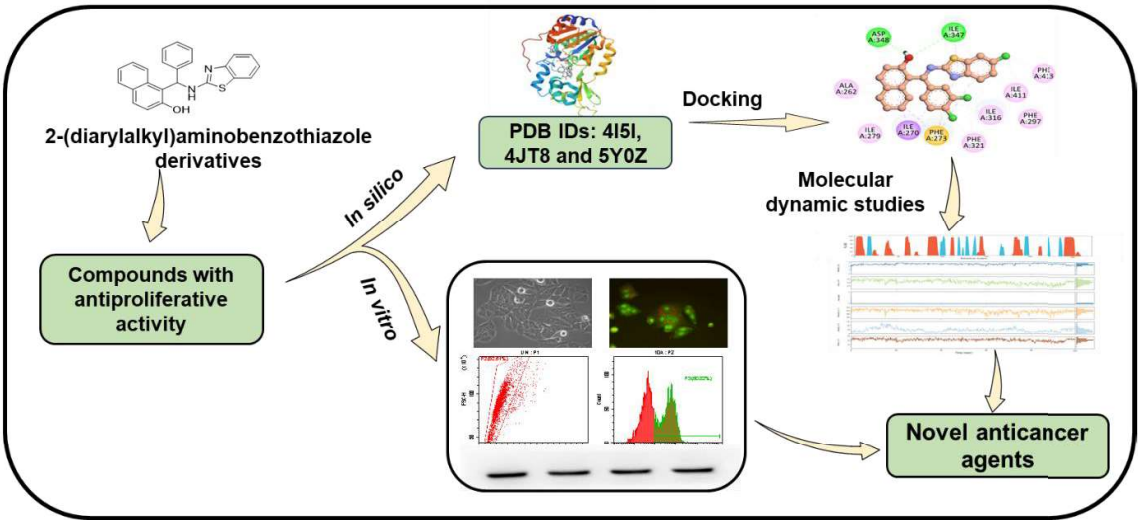

Figure 20: Graphical representation of workflow.

4.2 Materials and methods:

4.2.1 Synthesis of 2-(diarylalkyl)aminobenzothiazole derivatives:

The substrates, 2-aminobenzothiazole (1.0 mmol), Aldehyde (1.0 mmol), and β-naphthol (1.0 mmol) were each added to a 10 mL RB flask, which was subsequently heated in an oil bath that had been prepared to 110–120 °C for a period of 50 minutes. The reaction assortment was permitted to cool once the reaction was finished, as shown by TLC. This product was pulverized and rinsed with 3 x 8 mL of MeOH or EtOH to achieve the equivalent pure form of the 2-(diarylalkyl)aminobenzothiazole derivative [231].

4.2.2 Docking studies:

Autodock 4.2.6 was used for the docking studies [142]. The X-ray crystallographic structure of SIRT proteins 1-3 (PDB IDs 4I5I, 5Y0Z, and 4JT8) were chosen for their high resolution, lack of mutations, and applicability for complete similarity analysis. In line with other studies that demonstrate their significance in comprehending the structural and functional traits of particular SIRT family members, these structures offer reliable information for researching SIRT proteins [135-137, 232] with a precision of 2.6 Å was collected from the protein data bank of Research Collaboratory for Structural Bioinformatics (RCSB) (https://www.rcsb.org/) and retrieved in PDB format. The PDB has undergone removal of crystallographic water molecules and associated ligands. Further, the final protein structure of sirtuin after defrayal was preserved and saved as pdbqt format using AutoDockTools. The ChemDraw Professional software was used to design the ligand structures. Then, using the MM2 force field in Chem3D software, entirely the followed structures were energy-diminished, and pdb format were used to save the data files. Through Auto dock tools, total output archive files were stored as

pdbqt format. Further, fixed grid parameters were assigned to the pdbqt file that was directed by the amino acids from dynamic positions; SIRT-1 Chain A: Phe190, Phe180, Asp156, Phe131, Ala146, Pro140, Ala135, Phe119, Tyr139, Ile169, for the SIRT-2 Chain A the amino acid position: Ile347, Phe413, Phe297, Ile411, Asp348 and finally, for the SIRT-3 Chain A position of amino acids: Val298, His248, Asp231 were validated. Followed by the grid positions set as followed (X: 42.783, Y: -22.217, Y: 16.816) for SIRT1 protein, for SIRT2 the grid position parameters were set as (X: 13.127, Y: 49.067, Z: -27.711), and for the SIRT3 (X: 24.828, Y: 43.586, Z: -10.585) the grid position parameters were assigned. Similarly grid size followed for SIRT-1,2 and 3 proteins (X:56, Y:40, Z:40), (X:56, Y:50, Z:68) and (X:40 Y:40, Z:56) were validated [232]. No changes were made for docking parameters, all the parameters that were set as defaults and genetic algorithms were set to 100 runs and rest of the parameters was dispensed through docking Lamarckian genetic algorithm 4.2. Additionally, docking was performed in contrast to ligands with marked proteins (SIRTs 1-3). After successful completion of docking of ligand proteins, the obtained results were observed in analysis window of docking tools. Discovery studio visualizer 2021 client were used to analyze the docking results, the files were stored (BIOVIA 21.1.0). The reference compounds, EX-527 as SIRT1 inhibitor, SIRT2 inhibitor NPD11033, and SIRT3 inhibitor EX-A3489 were used to validate the docking parameters.

4.2.3 Molecular dynamic simulations of molecules 7ab and 7ba:

To examine the stability and binding interaction of docked ligands inside the recombinant active site of SIRT protein, molecular dynamics (MD) investigations were performed and the results analyzed using the Desmond program [233]. The investigations attempted to replicate physiological factors utilizing a solvated system in a cubic box containing 0.15 M NaCl and TIP3P water molecules. By utilizing NPT ensemble

conditions at 310 K temperature and 1 bar of pressure, MD simulations with periodic boundary conditions were performed. Before starting a simulation, the systems were relaxed and the simulations lasted at least 100 ns, and sometimes even 300 ns. To determine if the ligand was stable inside its binding pocket, the data were examined using root mean square deviation (RMSD) and root mean square fluctuation (RMSF) plots for the protein and ligand, respectively.

4.2.4 Molecular Mechanics Generalized Born and Surface Area (MMGBSA) calculations for molecules 7ab and 7ba:

To estimate the binding free energy for protein-ligand complexing, the MM-GBSA method was performed and executed using the Prime module in Schrödinger program (Schrödinger, LLC, New York), and it also provided the insights of energetics of system. The Continuous Solvent Generalized Born (VSGB) solvation model, which takes solvent effects into consideration, was used to improve this procedure [234]. The following formula was used to observe and calculate the protein-ligand total free energy binding.

$$Gcomplex - (Gprotein + Gligand) = dGbind$$

4.2.5 ADME, Drug likeness and toxicity predictions of molecules 7ab and 7ba:

The ADME properties of **7**ab and **7**ba were predicted using online server PreADMET (https://preadmet.webservice.bmdrc.org). Further drug likeness and toxicity parameters were predicted by using swissADME online server(www.swissadme.ch)[146].

4.2.6 Cell culture:

The cell line, MCF-7 (Breast cancer) was sourced from ATCC (Rockville, MD, USA). Cells were preserved and further grown in DMEM (Sigma St. Louis, MO) with

10% fetal bovine serum (Karlsruhe, Germany) and 1% antibiotics which included Kanamycin, and penicillin (Invitrogen, USA). The maintained parameters were 90% humidity and 5% CO2 at 37 ˚C. Cells were cultured until reached to confluence, further the cells were collected when reached to sub confluency, and plated accordingly with relevance to assays that need to be conducted.

4.2.7 Cytotoxicity study of 2-(diarylalkyl) aminobenzothiazole derivatives:

The sulforhodamine B assay was used to assess the cytotoxic potencies of the **7**ab and **7**ba compounds which were synthesized at CSIR-IICT. Briefly, 1×10^4 cells/well were plated in 96-well plate containing growth medium and allowed to grow overnight. Next day, culture growth medium was replaced with fresh medium. The test molecules at 1, 5, 10, 20, and 50 µM concentrations were added to cells, treated for 24 hours and cells treated with 0.5% v/v DMSO was used as control. After incubation period, cells were fixed with ice cold 50% w/v Trichloroacetic acid and allowed for incubation for 60 minutes at 4°C followed by gentle wash. After wash, 50 µL of SRB solution (0.04% w/v in 1% v/v acetic acid) was added to all the wells, followed by incubation for 60 minutes at room temperature. The excess dye was detached from the sample after staining by four times wash with 1% v/v acetic acid and allowed to dry. Then, 100 µL Tris base (10 mM, pH 10.5) was added to each and every well. Finally, absorbance reading was recorded at 490 nm using a microplate reader (Bio-Rad Laboratories, USA) and results were analyzed.

4.2.8 Cell morphology studies:

In six-well plates, about 1×10^5 cells/well MCF-7 cells were seeded. Further cells were allowed to grow at 37°C for 24 hours. The next day, cells were exposed to **7**ab and **7**ba at a concentration of 10 µM for 24 hours, with sirtinol (50 µM) serving as the positive

control. After incubation period, the cells were inspected using an inverted light microscope.

4.2.9 Acridine orange staining for detection of autophagy:

The acidic vesicular organelles (AVO) formed during autophagy induction were identified and assessed using acridine orange staining. Briefly, 1×10^5 cells/well MCF-7 cells were plated in six well plate containing growth medium, allowed to grow until cells reached 70% confluency. After that plates were replaced with fresh medium, and further treated with **7**ab or **7**ba at 10 μM or sirtinol (50 μM) for 24 h. After 24hr treatment period, 1 μg/ml acridine orange was used to stain the cells at 37 ˚C, 15 min. Then after, the excess staining was removed by washing with PBS, and cells were observed by fluorescence microscopy.

4.2.10 Clonogenic assay:

To assess the effect of molecules **7**ab and **7**ba on clonogenic survival, clonogenic assay was performed. Briefly, in six-well plates containing growth medium, the MCF-7 cells, 1×10^3 cells/well were seeded, then allowed to grow for 24hr. After incubation period, the cells were treated with molecules at 10 μM or sirtinol (50 μM) for 24 h. Further, the treated cells were allowed to grow for 12 days under conditions of 5% CO_2, 95% humidity at 37 ºC. Ethidium Bromide (10 μg/ml) was used to stain the colonies after they had been fixed in methanol for 30 minutes. The Image J software, an image processing application based on Java, was utilized to count the colonies.

4.2.11 Apoptosis determination by Annexin V/PI staining:

The molecules **7**ab and **7**ba were assessed for their potential to induce apoptosis in breast cancer cells. The cells were analyzed after treatment by annexin V/PI staining.

This was carried out by plating MCF-7 cells 2 × 10^5 cells/well in a 6-well plate and allowed for incubation overnight. Further, cultured cells were treated for 24 h with molecules at 10 μM or sirtinol (50 μM) and the control cells were 0.5% v/v DMSO treated. Next day, cells were washed with PBS to remove cellular debris, further they were resuspended in 100 μL of 1X binding buffer and stained with 1 μL of propidium iodide (PI; 100 μg/mL) and solution containing 5μL of Annexin V with conjugated Alexa Fluor 488 (Thermo Fisher Scientific, #V13241) were added and incubated for 15 minutes in a dark place. After 15 mins period, each sample was filled with 300 μL of 1X binding buffer and analyzed by flow cytometry (cytoFLEX, Beckman Coulter, USA; 488 nm laser).

4.2.12 Quantification of the intracellular ROS levels:

To investigate ROS induction in MCF-7 cells upon treatment with molecules, we performed flow cytometry using the ROS-sensitive probe 2',7'-dichlorodihydrofluorescein diacetate (C2938, DCFDA, Invitrogen, USA) to measure the amount of ROS within cells. Briefly, MCF-7 cells were seeded into a six well plate at a density of 1 × 10^5 cells/well and incubated in growth medium for overnight. Next day, **7**ab and **7**ba at 10 μM or sirtinol (50 μM) treatment was given to cells for 24 h, at 37 °C. After incubation period, 25 μM staining solution in PBS was added to cells and placed in the dark for 30 min at 37 °C, and directly analyzed using the flow cytometer (cytoFLEX, Beckman Coulter, USA; 488 nm laser).

4.2.13 Western blot analysis:

The MCF-7 cells, were seeded and incubated overnight in DMEM with 10% FBS and 1% antibiotics. Next day, **7**ab and **7**ba at 10 μM, sirtinol (50 μM) and DMSO were added to cells and treated for 24 h. The whole cell protein lysate was collected. Each

sample (40 μg) was run by PAGE electrophoresis using 10% SDS polyacrylamide gel. Further, the protein transfer from the gel to a polyvinylidene difluoride (PVDF) membrane was carried out. Five percent non-fat dried milk power dissolved in TBS + 0.1% Tween20 solution was used for blocking the membrane for two hours at normal room temperature. After blocking, the primary antibody was added and then incubated at 4 ˚C overnight. Further, to facilitate specific binding of antibody to protein, the membrane was rinsed 2-3 times with 1X TBST buffer solution for minutes. Further, the membranes were incubated with peroxidase conjugated secondary antibody dilution of 1:2000, (Santa Cruz Biotechnology, Texas, USA) for one hour at normal room temperature. Finally, the protein bands were observed using chemiluminescence detection system and bands were analyzed under the Chemi Doc XRS system (BioRad, Hercules, California, USA) with the expression of β-actin serving as the control.

4.2.14 Statistical analysis:

Each experiment was carried out in triplicate, and the results are shown as mean ± SD. Utilizing GraphPad Prism software version 5.01, statistical analyses were conducted. For multiple group comparisons, Tukey's post hoc test was utilized after one-way analysis of variance (ANOVA). P-values signify statistical significance (*$p < 0.05$, **$p < 0.01$, ***$p < 0.001$, $n = 3$).

4.3 Result:

4.3.1 Binding of 7ab and 7ba to SIRT 1,2 and 3 proteins:

We assessed the molecules, **7**ab and **7**ba SIRT protein binding ability by molecular docking studies. We observed that the two show better binding to SIRT1, 2 and 3 proteins with binding energies of -12.44, -12.08, 12.03 kcal/mol for **7**ab, and -12.07, -12.91, -11.86 kcal/mol for **7**ba respectively. The results were compared with the known inhibitors

EX-527 with binding energy of -10.26 kcal/mol for SIRT1, NPD11033 with binding energy of -11.19 kcal/mol for SIRT2 and EX-A3489 with binding energy of -10.73 kcal/mol for SIRT3 protein.

For SIRT1 of molecule **7**ab, we observed the following residues like ASP348, ILE347, PHE273, PHE297, PHE413, ILE411, ILE279 and ILE316 were similar with standard. For molecule **7**ba, the residues like ILE347, ILE279, ILE316, ILE411, PHE297, and PHE273 were similar with standard. Molecule **7**ab forms ILE347 and ASP348 conventional hydrogen bond, the Pi-Sigma bond interactions with ILE270, while PHE273 forms the Pi-Sulfur interactions and PHE321, ILE316, ILE411 and PHE413 displayed Alkyl and Pi-Alkyl interactions. The **7**ba forms the Pi-Sigma interactions with ILE347, and PHE273 Pi-Sulfur interaction, Pi-Pi T shaped bond with PHE297 and PHE321, ILE316, ILE411 forms the Alkyl and Pi-Alkyl interactions. The EX-527 forms the hydrogen bond with ILE347, ASP348 and PHE273 and PHE297 displayed Pi-Pi T shaped interactions and ILE279, ILE316, ILE411 forms Alkyl and Pi- Alkyl bonds (Figure 21).

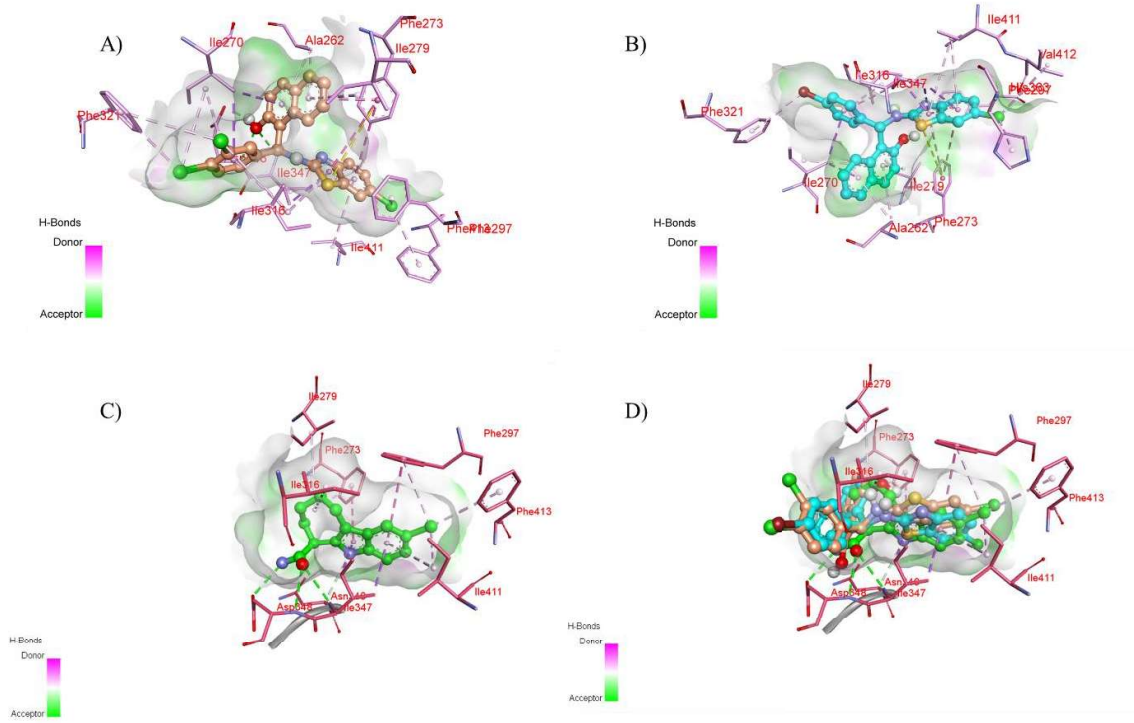

Figure 21: Binding interaction of molecules **7**ab and **7**ba and reference compounds at SIRT1 active sites. A), B) and C) represents binding interaction of **7**ab**,** **7**ba and reference compound EX-527, and D) represents superimposed position of ligands at the active site of SIRT1(Gold color: **7**ab, pastel blue color: **7**ba, green color: EX-527 reference compound)

For SIRT2 of molecule **7**ab, residues like ARG97, ALA85, ALA135, ILE93, ILE169, PHE96 and PHE119 were common compared with standard. For the molecule **7**ba, ALA85, ALA135, ILE93, ILE169, PHE96 and PHE119 were similar with standard. The molecule **7**ab, forms the conventional hydrogen bond with ARG97 and PHE96, Pi-Pi stacked, Pi-Pi T shaped bonds PHE119, PHE235. LEU103, LEU138, ALA135, and PHE131 forms the Alkyl and Pi-Alkyl interactions. For the molecule **7**ba, Phe96 forms the conventional hydrogen bond interactions, PHE235 and PHE119 showed Pi-Pi, Pi-Pi T shaped interactions, and Alkyl, Pi-Alkyl bonds were displayed LEU134, PHE131,

ALA135. NPD11033 showed Pi-Pi T shaped interactions PHE96, PHE190 while ALA135, ALA85, ILE93, ILE169 forms the Alkyl and Pi-Alkyl interactions (Figure 22).

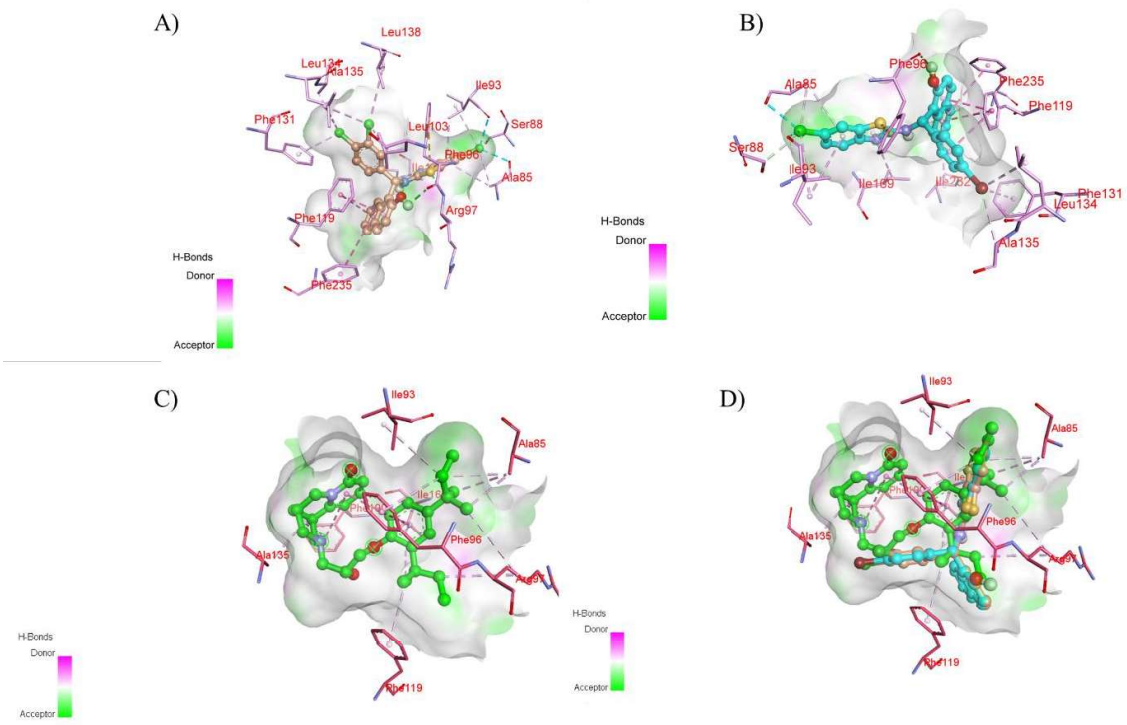

Figure 22: Binding interaction of molecules **7**ab and **7**ba and reference compounds at SIRT2 active sites. A), B) and C) represents binding interactions of **7**ab, **7**ba and reference compound NPD11033, and D) represents superimposed position of ligands at the active site of SIRT2 (Gold color: **7**ab, pastel blue color: **7**ba and green color: NPD11033 reference compound)

For SIRT3 the molecule **7**ab, we observed ALA146, GLN228, HIS248, ILE230, SER149, PHE157, and PHE294 were similar to standard. For molecule **7**ba, ALA146, HIS248, ILE230, PHE157 and PHE180 showed better binding interactions with standard. The molecule **7**ab, made the interaction bonds like conventional hydrogen bond with GLN228, halogen bonds with ARG158, unfavored bond with HIS248, Pi-Sigma bond

with ASN229, PI-stacked and Pi-Pi T shaped bonds PHE157, PHE294 and Alkyl, Pi-Alkyl bonds ALA146, ILE154 and TYR165. For the molecule 2 Pi-cation bond formed with ARG158, Pi-Sigma bond with ALA146, Pi-Pi stacked with HIS248 and PHE157, Alkyl and Pi-Alkyl interaction with ILE230, ILE291 and PHE180. Whereas the EX-A3489 forms the carbon hydrogen bond with ASP156, GLN228 and SER149, Pi-Sigma bond with ALA146, Pi-Pi stacked PHE157, Alkyl, Pi-Alkyl interaction HIS248, ILE230, PHE180 and PHE294 (Figure 23).

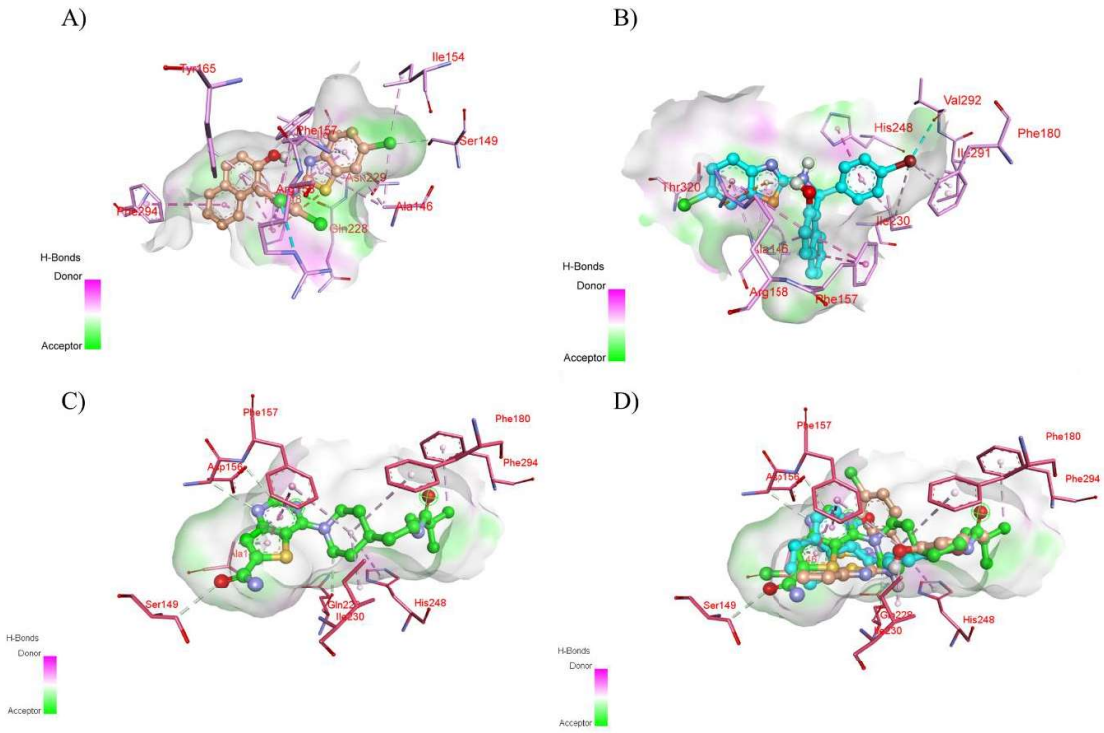

Figure 23: Binding interaction of molecules **7**ab and **7**ba and reference compounds at SIRT3 active sites. A), B) and C) represents binding interaction of **7**ab, **7**ba and reference compound EX-A3489, and D) represents superimposed position of ligands at the active site of SIRT3 (Gold color: **7**ab, pastel blue color: **7**ba and green color: EX-A3489 reference compound)

4.3.2 Molecular dynamic simulation studies on SIRT1:

Molecular dynamic simulation studies were performed to analyze the mode of binding and interaction stability of **7**ab, **7**ba and EX-527with SIRT1. The overall stability of 7ab, 7ba and EX-527 with SIRT1 simulation was analyzed using the root mean square deviations (RMSD), the ligand root mean square fluctuation (L-RMSF) of the backbone atoms. The RMSD graph plot suggests that molecules **7**ab,**7**ba and EX-527 form the stable interaction throughout the stimulation with protein backbone atoms (Figure 24).

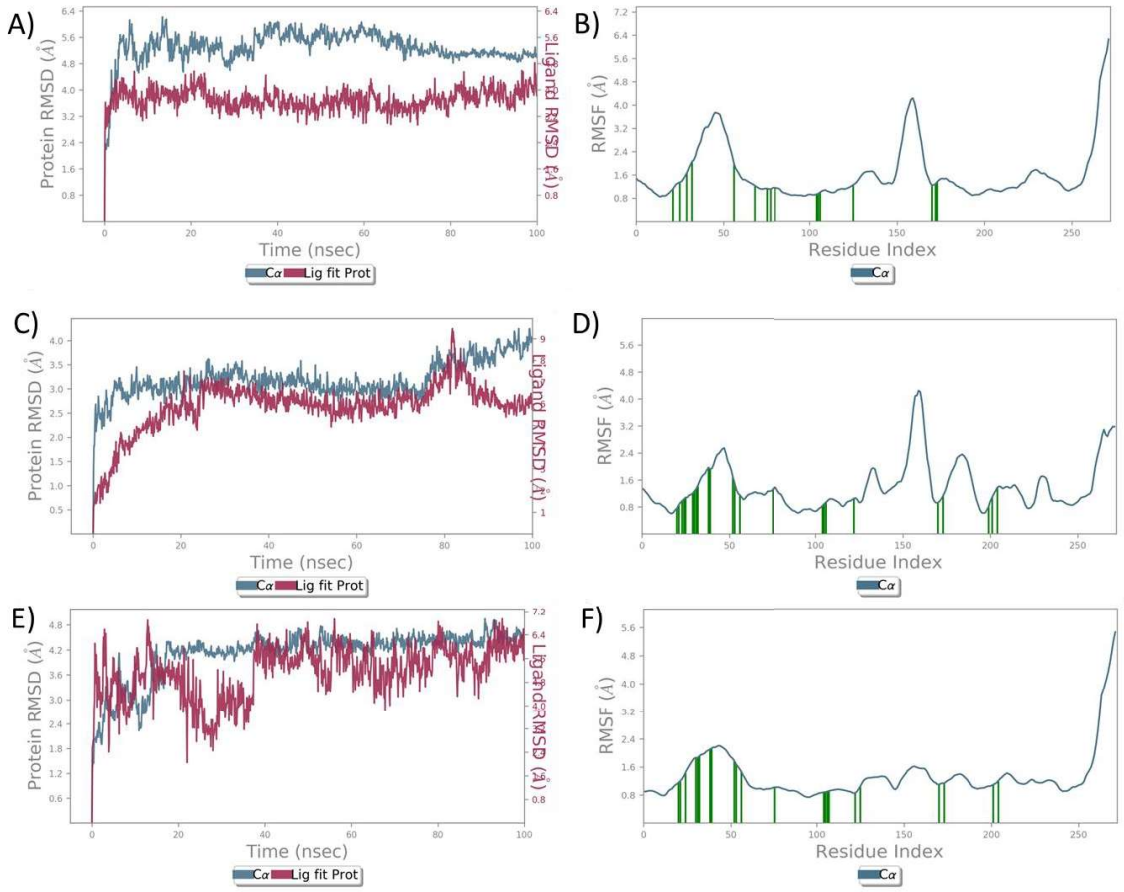

Figure 24: Binding interaction of molecules **7**ab, **7**ba and EX-527 with SIRT1 molecular dynamic simulation, A) and B) are RMSD and RMSF of molecules **7**ab, C) and D) are RMSD and RMSF of molecule **7**ba and E) and F) are RMSD and RMSF of reference compound EX-527.

Furthermore, the protein-ligand interactions of **7**ab, **7**ba and EX-527 were analyzed. The hydrogen bond interactions of **7**ab with SIRT1 involved Gln345, Asn346, and Ile347 which resembles the drug specificity, absorption and metabolism. Ala262, Val266, Ile270, Phe273, Phe297, Phe309, Ile316, Pro318, Phe366, Ile411, Phe414 were part of the hydrophobic interactions and no ionic and water bridges were observed. The following hydrogen bond interactions were noticed for 7ba with SIRT1 at Val264, Pro271 and Ile279. The hydrophobic bonds were at Val266, Asp272, Ile279, Gln294, Phe297, Asn346, Ile411, Val445 and ionic bonds were at Ile316, Ser442. The water bridges were observed at Gly261, Val264, Ile270, Pro271, Ile279, Tyr280, Pro293, Ile316, Gln345, and Ile 347. The following hydrogen bonds Ile316, Gln345, Asn346, Ile347, and Asp348 were observed for EX-527. The hydrophobic interaction Asp272, Gln294, Phe366 and Ile411 were observed and ionic interactions Gly261, Ala262, Ser265, Gln345, and Ile347 were observed. Furthermore, the water bridges Gly261, Ala262, Ser265, Asp272, Ile279, Phe297, Ile316, Gln345, Asn346, and Ile347 were observed for EX-527. The observed results suggest that 7ab and 7ba stable at sirt1 compared with reference EX-527 (Figure 25).

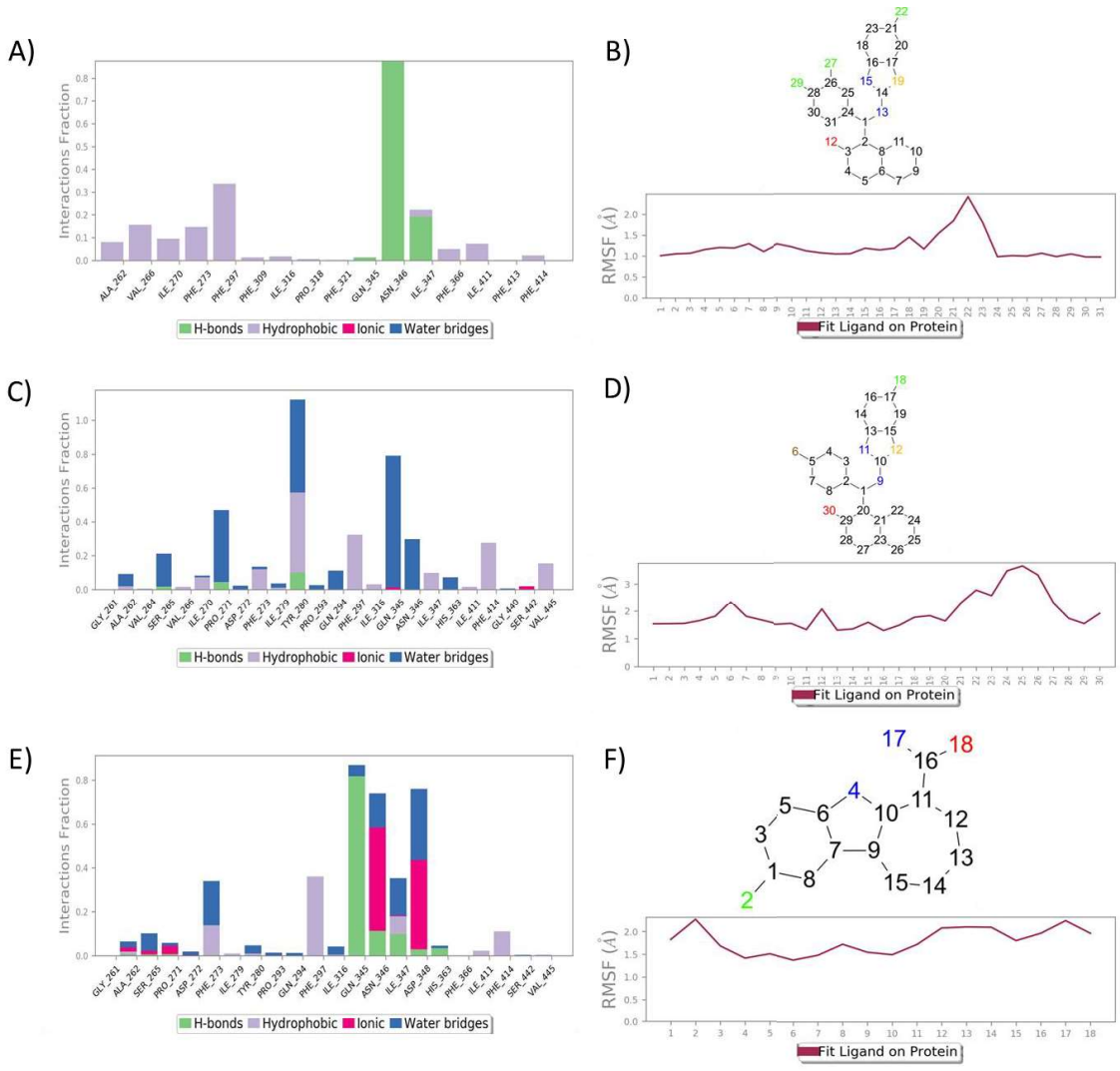

Figure 25: Protein-ligand interactions by molecular dynamic simulation, A) bar chart of **7**ab, B) protein ligand RMSF interactions of **7**ab throughout simulation, C) bar chart of **7**ba, D) protein-ligand RMSF interaction of **7**ba, E) bar chart of reference EX-527 and F) protein-ligand RMSF interaction of EX-527.

4.3.3 Analysis of Molecular Mechanics Generalized Born and Surface Area (MMGBSA) of molecules 7ab and 7ba:

The MMGBSA is an approach that provides rapid and efficient analysis for determining the stability and strength of interactions of the protein-ligand complex binding free energy in molecular simulations. Molecules **7**ab and **7**ba with Sirt1 protein

complex of non-bonded interaction as well as the binding free energies were analysed. The dGbind values of 7ab, 7ba and EX-527 were -68.11, -56.88 and -52.96 (kcal/mol). Further, dG_{bind}Lipo, dG_{bind}Hbond, dG_{bind}vdW, were analyzed and the result of binding energies data provided the support for the simulation and docking data (Table 4).

Table 4. Calculations of dG bind values of 7ab and 7ba with SIRT-1 by MM-GBSA binding energy MD Simulation.

Energies (kcal/mol)	SIRT1		
	RN7AB	RN7BA	EX-527
dG_{bind}	-68.11507899	-56.88863734	-52.96735947
dG_{bind}Lipo	-33.53673621	-31.40320527	-27.32073522
dG_{bind}vdW	-64.17783634	-53.24302506	-47.53808588
dG_{bind}Coulomb	-13.68895096	-9.627138559	-13.1166964
dG_{bind}Hbond	-1.03758685	-0.246628598	-0.473347814
dG_{bind}Packing	0	0	0

4.3.4 Study of ADME, drug-likeness and toxicity predictions:

The molecules 7ab and 7ba were evaluated through swissADME and preADMET online servers. The observed results showed 7ab and 7ba obeying Lipinski's rule of 5 drug likeness parameters, furthermore, ADME and toxicity predictions revealed less penetration through BBB, no toxicity on rodents and hERG prediction indicates medium risk to cardiotoxicity and the obtained results were tabulated and accessible as a supplementary file.

4.3.5 Molecules 7ab and 7ba inhibit proliferation of MCF-7 cells:

The molecules 7ab and 7ba were tested for their anticancer potencies against MCF-7 breast cancer cell line by sulforhodamine B assay. These molecules showed potent antiproliferative effect on MCF-7 cell line in a dose dependent manner for 24h (Figure 26). As shown in cell viability graph of MCF-7 cell line, at 10 µM concentration we

observed almost 50% growth inhibition. The cytotoxicity assay involved assessing the derivatives 7ab and 7ba on normal human embryonic kidney cells as well and we did not find any cytotoxicity on normal cell line up to 100 micromolar of 7ab and 7ba. To study the long-term effect of **7**ab and **7**ba on cell survival we performed clonogenic assay at 10 µM. We observed a reduction in the total number of colonies formed, indicating an impact on the cellular survival of MCF-7 cells as compared to non-treated cells (Figure 26). These results suggest that molecules **7**ab and **7**ba have inhibitory effect on cell colony formation and confirm long term inhibitory effect on breast cancer cell proliferation.

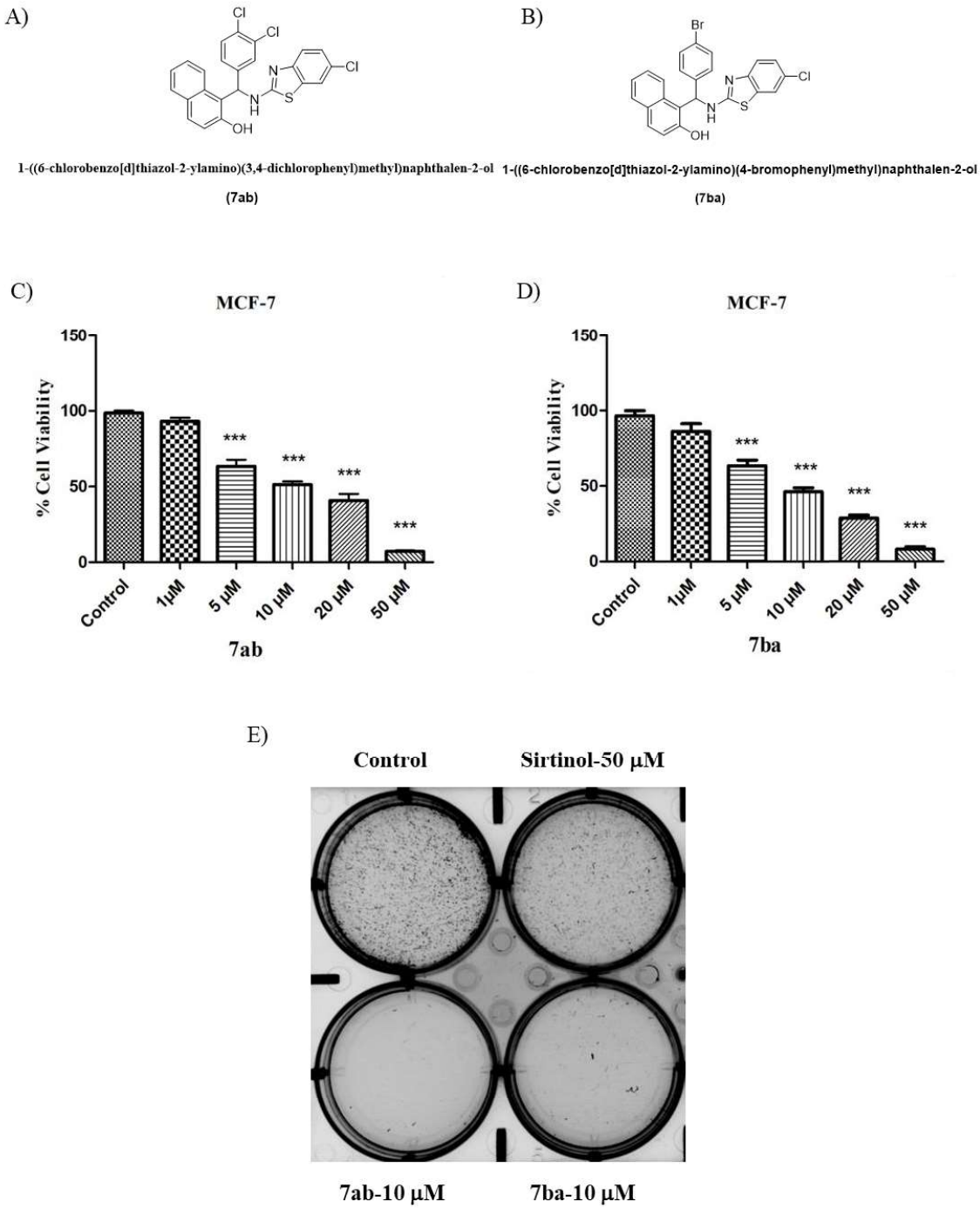

Figure 26: Molecules 7ab and 7ba inhibit the cell proliferation and colony formation in MCF-7 cancer cell line. A) and B) are chemical structures of molecules 7ab and 7ba, C) and D) percentage cell viability after treatment with 7ab and 7ba in MCF-7

cell lines, and E) shows effect on colony formation after the treatment with **7**ab and **7**ba in MCF-7 cell lines

4.3.6 Molecules 7ab and 7ba inhibit SIRT protein expression and alter the expression levels of p53 and Bcl-2 in MCF-7 cells:

Based on docking results, which showed stronger binding of **7**ab and **7**ba to SIRT1, SIRT2, and SIRT3 proteins, we next evaluated the SIRT-inhibitory effects using Western blot analysis in MCF7 cells. Our findings revealed that treatment with **7**ab and **7**ba at 10 μM resulted in a significant reduction in the expression of SIRT1, SIRT2, and SIRT3 compared to the control and sirtinol (50 μM), a known positive control for SIRT inhibition. We also assessed the acetylation of p53, a downstream target of SIRT1, and observed a marked decrease in acetylation at lys382. This led to an increase in both total p53 expression and its activation. The activation of p53 appears to drive antiproliferative and pro-apoptotic effects, enhancing the expression of pro-apoptotic factors while decreasing the levels of anti-apoptotic proteins such as Bcl-2. Furthermore, in addition to activating p53, treatment with **7**ab and **7**ba led to a decrease in Bcl-2 expression (Figure 27).

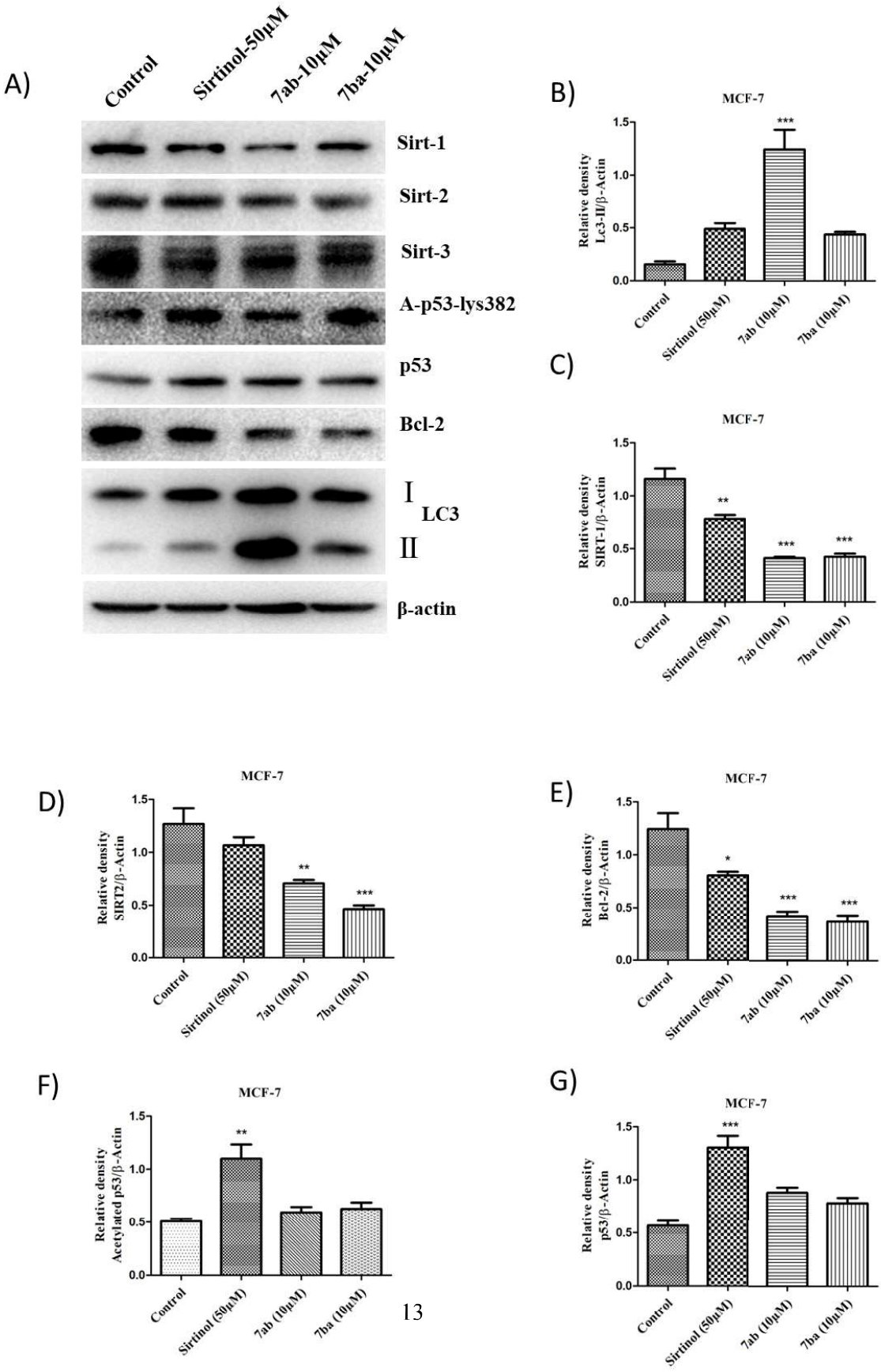
A)
Control
Sirtinol-50μM
7ab-10μM
7ba-10μM
Sirt-1
Sirt-2
Sirt-3
A-p53-lys382
p53
Bcl-2
I
LC3
II
β-actin
B)
MCF-7
Relative density Lc3-II/β-Actin
C)
MCF-7
Relative density SIRT-1/β-Actin
D)
MCF-7
Relative density SIRT2/β-Actin
E)
MCF-7
Relative density Bcl-2/β-Actin
F)
MCF-7
Relative density Acetylated p53/β-Actin
G)
MCF-7
Relative density p53/β-Actin
Control
Sirtinol (50μM)
7ab (10μM)
7ba (10μM)

Figure 27: Molecules **7**ab and **7**ba decrease Sirtuins expression. A) Western blots showing relative protein expression levels of SIRT 1, SIRT 2, SIRT 3, Apoptosis related proteins- p53, acetylated p53, and Bcl2, autophagic protein LC3 with that of beta-actin, B) and C) relative density of LC3-II and SIRT1, D) and E) relative density of SIRT2 and Bcl-2, F) and G) relative density of acetylated p53 and p53 protein expression levels in MCF-7 cells treated with sirtinol-50 μM (Positive control), with that of β-actin, **7**ab-10 μM and **7**ba-10 μM (± SD, ANOVA where, n = 3 [*P < 0.05, **P < 0.01, ***P < 0.001]).

4.3.7 Molecules 7ab and 7ba induce ROS dependent apoptosis in MCF-7 cells:

To assess whether the cytotoxic effects of 7ab and 7ba are due to apoptosis, MCF-7 cells treated with **7**ab and **7**ba at 10 μM concentration for 24h were evaluated for cell death using the Annexin V/PI assay. We observed that percentage of apoptotic cell population significantly increased in **7**ab (48.84%) and 7ba (36.99%) treated cells as compared to control and sirtinol (22.16%) treatment (Figure 28A).

Intracellular oxidative stress due to ROS production plays important role in the induction of apoptosis. Therefore, we further investigated whether **7**ab and **7**ba could stimulate ROS generation in MCF-7 cells, we detected ROS induction by staining cells with DCFDA and analyzed using flow cytometric analysis. The molecules 7ab and 7ba showed induction of reactive oxygen species levels in treated cells as compared to control cells (Figure 28B). These results suggest that **7**ab and **7**ba induced apoptosis is due to accumulation of intracellular ROS in MCF-7 cells.

We observed that the late-stage apoptosis percentage cell population was significantly increased compared with control. Further analysis of anti-apoptotic marker Bcl-2 protein expression showed decline in Bcl-2 expression compared to control cells (Figure 27).

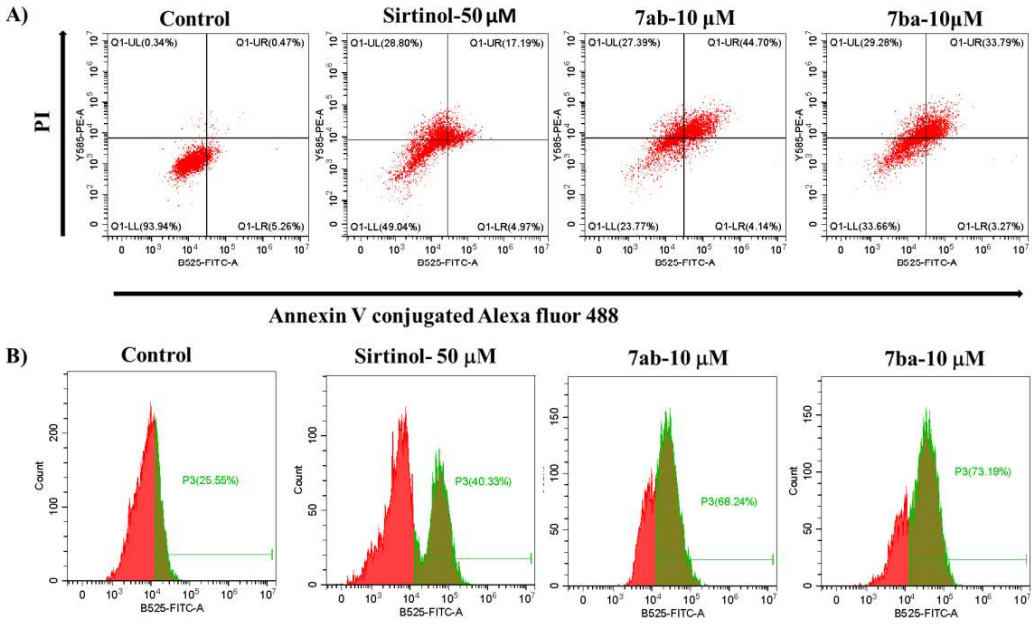

Figure 28: Molecules 7ab and 7ba induced apoptosis and ROS in MCF-7 cell line. A) Representative images of Annexin V-FITC assay of MCF-7 cells treated with sirtinol-50 µM, 7ab-10 µM and 7ba-10 µM, B) ROS formation in MCF-7 cells untreated (control), treated with sirtinol-50 µM, 7ab-10 µM and 7ba-10 µM.

4.3.8 Molecules 7ab and 7ba induce autophagy in MCF-7 cancer cells:

The MCF-7 cell line was treated with either 7ab or 7ba at concentrations of 10 µM for 24hr and sirtinol (50 µM) served as positive control. The morphology of cells was observed under light microscope which displayed formation of vacuoles in the cytoplasm (Figure 29A). The results suggest that treating the MCF-7 cell line with 7ab and 7ba induces autophagy in these cells. Further, we confirmed this with acridine orange staining.

In general, acridine orange exhibits green fluorescence at neutral pH, but in an acidic vacuole, it exhibits orange-red fluorescence. Comparing treatment with control cells, we saw that the orange-red fluorescence of these molecules indicated acidic vacuolar organellar formation (Figure 29B). The conversion of a soluble protein form

LC3-I to LC3-II by phosphatidylethanolamine (PE), which is associated with autophagic vesicles, is a clear indication of autophagosome development. After being treated with the molecules 7ab and 7ba (10 µM) for 24 hours, we observed an increase in LC3-II expression, which suggests that these molecules can enhance the production of autophagosomes (Figure 27). These findings collectively imply that molecules 7ab and 7ba cause MCF7 cells to undergo autophagy.

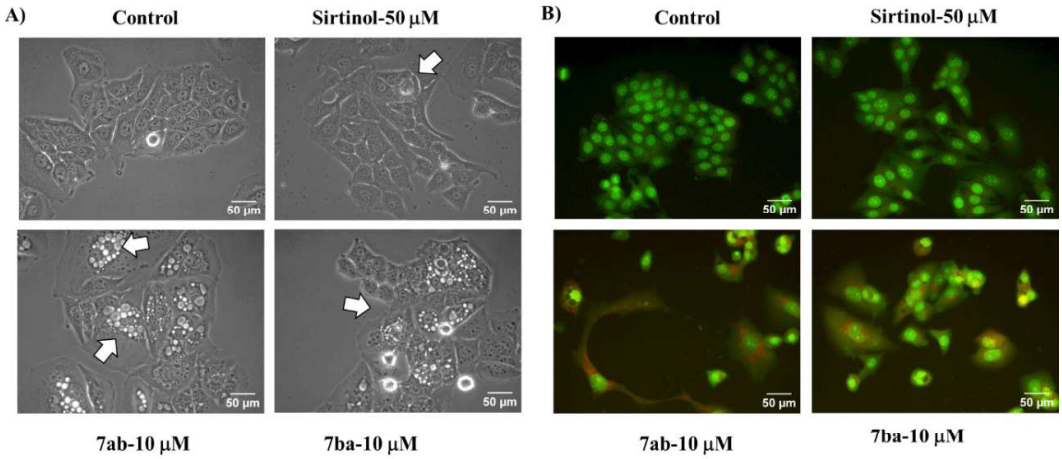

Figure 29: Molecules 7ab and 7ba induce acidic vacuoles formation in MCF-7 cell line. A) Cell morphology of MCF-7 cells treated with sirtinol-50 µM, 7ab-10 µM and 7ba-10 µM. B) AVO formation in MCF-7 cells treated with sirtinol-50 µM, 7ab-10 µM and 7ba-10 µM. Orange-red color represents AVO formation.

4.4 Discussion:

Sirtuins (SIRTs) are distinct proteins that are known to control phases of metastasis, carcinogenesis, and the emergence of multidrug resistance [235]. SIRT 1, 2 and 3 belong to class 1 SIRTs as indicated by molecular pathological analysis [147]. The overexpression of SIRTs is reported in breast cancer and known to play critical role in cell proliferation, differentiation, apoptosis, invasion, and metastasis. Therefore,

inhibiting SIRT proteins would have better anticancer potencies in breast cancer [236]. In this investigation, we assessed the anticancer potential of 2-(diarylalkyl) amino benzothiazole derivatives **7**ab and **7**ba and underlying molecular mechanisms of action on breast cancer cells. We first established that **7**ab, **7**ba exhibit potent anti-cancer activities and then explored that these molecules are possibly showing the action by acting as SIRT inhibitors.

In current study, we utilized MCF-7 breast cancer cells due to their high expression of SIRT1 and both SIRT1 and SIRT2 may acetylate functional p53. The tumor suppressor protein p53 plays a crucial role in controlling cell growth, inducing apoptosis, and promoting cellular senescence in response to different stress factors [237]. We observed decrease in cell viability and colony formation in MCF-7 cells upon treatment with **7**ab and **7**ba (Figure 26).

Docking studies were performed for **7**ab and **7**ba against SIRT1/2 and 3 proteins. We found that **7**ab and **7**ba displayed better binding energies compared to known reference inhibitors against SIRTs. Additionally, molecular dynamic simulation studies revealed promising and better binding interactions with SIRT1 protein. Since most cell cycle proteins and death regulators are found in the same intracellular compartments as SIRT1, it plays a more significant role in regulating cellular growth and cell survival [238]. This enables SIRT1 to directly interact with these regulators and modify their activity, which in turn affects cellular processes including autophagy, apoptosis, and the advancement of the cell cycle [239].

Following the in-silico study, we performed in vitro experiments with **7**ab and **7**ba to examine their effects on inhibiting SIRT activity. As expected, we observed that the molecules **7**ab and **7**ba decrease SIRT1, moderately reduce SIRT2 and SIRT3 protein

expression, with increase in acetylation and activation of p53 compared to control (Figure 27). The activation of p53 seems to promote antiproliferative and pro-apoptotic effects by increasing pro-apoptotic factors and reducing the levels of anti-apoptotic proteins like Bcl-2. We also observed treatment with **7**ab and **7**ba not only activates p53 but also results in a reduction of Bcl-2 expression (Figure 27).

We further explored the mechanism behind anticancer effects of these molecules. Therefore, autophagy and apoptosis cell death were assessed. We assessed apoptosis in MCF-7 cells upon treatment with **7**ab and **7**ba. By performing Annexin V-PI staining followed by flowcytometry we observed increase in the percentage of apoptotic cell population upon treatment compared to control MCF-7 cells (Figure 28A). We also observed increased ROS levels in treated MCF-7 breast cancer cell line compared to control cells. These findings suggest that **7**ab and **7**ba induced apoptosis is ROS dependent (Figure 28B). We also observed vacuole formation in the cytoplasm following treatment with **7**ab and **7**ba in MCF-7 cells. To further confirm autophagy, we performed acridine orange staining to detect AVO formation which is one of the crucial determinants for autophagy induction. We observed that treatment with **7**ab and **7**ba reported more abundance of AVOs compared to control (Figure 29). Furthermore, we confirmed autophagy by measuring the expression of the protein LC3-II, which was increased upon treatment in MCF-7 cells compared to control (Figure 29).

In summary, our findings indicate that **7**ab and **7**ba reduce the expression of SIRT proteins, activate p53, and trigger apoptosis, while also promoting autophagic cell death.

4.5 Conclusion:

In conclusion, current study confirmed that molecules **7**ab and **7**ba cause cytotoxic effect in human breast cancer cells by inhibiting SIRTs leading to deacetylation and

activation of p53 in MCF-7 cells. Molecules **7**ab and **7**ba induce autophagic and apoptotic cell death. Overall, the study indicates that the molecules **7**ab and **7**ba are potential cytotoxic agents and effective SIRT inhibitors and therefore, can be further considered or explored towards development of novel molecules as potential anticancer agents for breast cancer treatment.